Stabilities of amorphous indium gallium zinc oxide thin films under light illumination with various wavelengths and intensities

2014 Jpn. J. Appl. Phys. 53 08NG03

(http://iopscience.iop.org/1347-4065/53/8S3/08NG03)

Japanese Journal of Applied Physics **53**, 08NG03 (2014) **REGULAR PAPER**
http://dx.doi.org/10.7567/JJAP.53.08NG03

Stabilities of amorphous indium gallium zinc oxide thin films under light illumination with various wavelengths and intensities

Ju-Yeon Kim[1], So Hyeon Jeong[1], Kyeong Min Yu[1], Eui-Jung Yun[1,2], and Byung Seong Bae[1*]

[1]*Department of Display Engineering, Hoseo University, Asan, Chungnam 336-795, Republic of Korea*
[2]*Department of System Control Engineering, Hoseo University, Asan, Chungnam 336-795, Republic of Korea*
E-mail: bsbae3@hoseo.edu

Received January 15, 2014; accepted May 19, 2014; published online July 10, 2014

We investigated the photo responses of an amorphous indium gallium zinc oxide (a-IGZO) thin film under light illumination with various wavelengths and intensities. By using the measured photo-conductivities of a-IGZO thin films, we extracted the photo excitation activation energy and dark relaxation activation energy through extended stretched exponential analysis. The stretched exponential analysis was found to describe well both the photoexcitation and the dark-relaxation characteristics. These analyses indicated that recombination takes place more slowly and through activation processes that are more deeply bound with the broader distribution of activation energies (E_{ac}) than those corresponding to the photo-generation process. The longer wavelength of the incident light, the slower the dark-relaxation occurs because of the formation of higher E_{ac} for the ionized oxygen vacancy (V_o^{2+}) states. For the dark-relaxation process, we also observed that the stretching exponent increases and the distribution of energy levels became narrower for longer wavelengths. This suggests that the neutralization of V_o^{2+} to V_o is slower for longer wavelengths due to the higher energy barrier height (E_{ac}) for the neutralization of V_o^{2+}. © 2014 The Japan Society of Applied Physics

1. Introduction

Recently, amorphous oxide semiconductors (AOSs) have attracted much attention because these materials can be used as active channels in thin-film transistors (TFTs).[1–10] They have several merits compared to amorphous silicon TFTs, such as their direct wide-band gap, good transparency, and higher mobility.[11,12] Their high mobility is attributed to the ionic bonding nature of Zn-based oxides. The AOSs are particularly useful compared to hydrogenated amorphous silicon (a-Si:H) because the Fermi level can be stably shifted above the mobility edge by the gate voltage; therefore, the much higher value of the free carrier concentrations is possible for AOSs compared to a-Si:H.[9–14] In terms of the sub-gap states, it has been indicated by optical measurements that the deep levels in AOSs are induced by the oxygen vacancy (V_o) defects.

Stability and gap states have been the main research themes from the early stages of the development of oxide TFTs.[12,15–18] Many researchers have reported on the sub-gap density of states (DOS) for amorphous indium gallium zinc oxide (a-IGZO) TFTs; however, combined and unified models have not yet been established.[4] Although many research studies that examined a-IGZO TFTs have reported on the stability of a-IGZO, their analyses were complex and limited due to the presence of interfaces related to the active channel, gate insulator, and source–drain electrodes.

The photo responses that are involved in the photo excitation and dark-relaxation phenomena of a-IGZO thin films were investigated under light illumination with various wavelengths and intensities, and an energy band diagram of the sample was deduced.

2. Experimental procedure

The a-IGZO thin films were sputter-deposited on bare glass. The partial pressures of argon and oxygen reaction gases were 0.2 and 0.5 mTorr, respectively. After deposition of the a-IGZO thin film, Al electrodes were deposited on the a-IGZO thin film using the thermal evaporator at a pressure of 10^{-6} Torr. The width and length of the Al electrodes were 1500 and 100 μm, respectively. The thickness of both the a-IGZO thin film and the Al electrode were around 100 nm. To avoid the effect of moisture and other impurities, the measurements were conducted in a vacuum chamber. We measured the photocurrents of a-IGZO thin film for an hour at a temperature of 333 K. After we turned off the light source, the dark relaxation currents were monitored for an hour. In order to have the original state after measurement, we annealed all samples for an hour at a temperature of 180 °C. The three different LED light sources with wavelengths of 400, 530, and 850 nm were used. For the investigation of the intensity dependency, three different intensities of 0.2, 0.3, and 0.4 mW/cm^2 for the 400 nm LED light source were employed. All the currents were measured at an applied voltage of 1 V.

The stretched exponential analyses were carried out as follows: The characteristics of photocurrents versus time (I_{ph}–t) were analyzed with a stretched exponential function of

$$I_{ph} = \frac{(\sigma(t) - \sigma_s)VWt_{ch}}{L} = \left(\frac{\sigma_{ph0}VWt_{ch}}{L}\right)\exp\left[-\left(\frac{t}{\tau}\right)^{\beta}\right]. \quad (1)$$

Here, $\sigma(t)$ is the time-dependent sample conductivity, σ_s is the saturated photo-conductivity at long times, σ_{ph0} is the weighting amplitude of photoconductivity, V is the bias voltage, t_{ch} is the thickness of the a-IGZO thin films, W is the width of the sample, L is the length of the sample, τ is the effective time constant, and β is the stretching exponent.

The incident photon flux (N_{ph}) can be obtained by using the relation of

$$N_{ph} = \frac{P_\lambda}{E_{ph}}. \quad (2)$$

Here, P_λ is the power of the incident light per unit area with a wavelength λ, and E_{ph} is the energy of the incident photons.

We obtained fitting parameters such as β, τ, E_{ac}, and Δ_{ac} for all the measured data from the stretched exponential analysis. The activation energy E_{ac} and the activation energy bandwidth Δ_{ac} were calculated by these expressions as follows:

$$E_{ac} = E(t) = k_B T \ln(t\nu), \quad (3)$$

$$\Delta_{ac} = 4.6(\beta^{-0.81} - 1)k_B T. \quad (4)$$

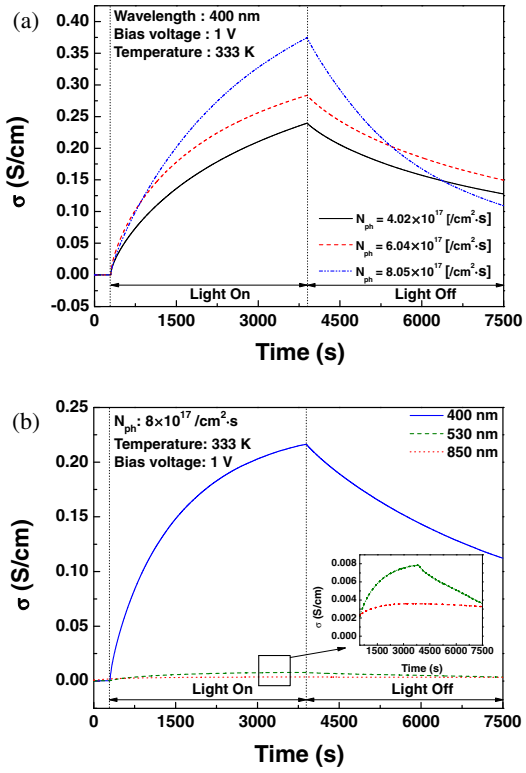

Fig. 1. (Color online) Comparison of photo- and dark-relaxation of conductivities as a function of (a) the flux of incident photons (N_{ph}), and (b) the wavelength of incident lights.

Here, E_{ac} is the central value of the activation energy, Δ_{ac} is the full width at half the maximum of the activation energy distribution, k_B is Boltzmann's constant, T is the sample temperature, t is the experiment time, and ν is the attempt-to-escape frequency. E_{ac} was calculated from Eq. (3) assuming $\nu = 10^{13}$ Hz and $t = \tau$.[19,20] Following the authors,[11,20] Eq. (4) was deduced as a simple empirical equation. It fits the calculated Δ_{ac} to within 8% and provides a quick way to estimate the Δ_{ac} for any β in the range $0.05 < \beta < 1$. We extracted the photo excitation and dark-relaxation activation energies through extended stretched exponential analysis.

3. Results and discussion

The time-dependence of the photo and dark relaxation conductivities as a function of the photon flux and the wavelength of incident lights is shown in Fig. 1. In general, the photocurrent of the semiconductor increases sharply under illumination; however, the measured photocurrents for the samples prepared in this study show a slow increase during illumination. These slow increases of the photocurrent indicate that the density of the free carriers increase during illumination, which is attributed to the increase of donor states (ionized oxygen vacancies; V_o^{2+}), based on the many research results reported in the current literature.[11,19,21] As shown in Fig. 1, the photocurrents increase as the incident photon flux (N_{ph}) increases, and the wavelength of incident lights (λ) decrease, indicating an increase in V_o^{2+} states with a higher N_{ph} and shorter λ. The stretched exponential analysis was also found to describe well both the photoexcitation and dark-relaxation characteristics of a-IGZO thin films and TFTs.[11,19] Thus, we analyzed the experimental results using the stretched exponential technique.

Figure 1(a) shows the photoexcitation and dark relaxation of the conductivities as a function of the photon flux. Once the light is turned off, the conductivities of the a-IGZO thin films did not immediately recover to their original states, but decreased slowly and they show a persistent photoconductivity (PPC), which was also observed by other research groups.[20,22] Since the photo carriers can be induced from the donor levels such as V_o^{2+}, we suggest that the slow decrease of the dark current can be attributed to the slow neutralization of V_o^{2+}. It was reported that V_o^{2+} can generate photo-carriers and form metastable states.[19,23–27]

The inset in Fig. 1(b) shows the photoconductivity of two λs of 530 and 850 nm. For the photoexcitation data for a λ of 850 nm, the photoconductivity saturated shortly to the σ_s of 0.0036 S/cm during irradiation, and the dark-relaxation rates after the irradiation was turned off were very slow compared to those for the shorter wavelengths. The photo-currents were saturated when the equilibrium between the photo-generation from and recombination to the deep states or tail states of V_o takes place during the light irradiation. For the low photon energy of 1.46 eV, the weak photocurrent will saturate rapidly due to the ionization of the V_o with a low density. The oxygen vacancies, which can be excited, are just the ones distributed around the top among the vacancies distributed in the band gap. Vacancies distributed at upper energies are few compared to those at the middle part, the excitation by low energy irradiation is limited to a short time; therefore the photo current saturated quickly.

Furthermore, with the low excitation energy, it is more likely that the electrons are excited to the tail states located close to the bottom of the conduction band, which results in the slow recovery of the dark relaxation with a non-exponential fashion at the early stage after the light was turned off. This is because the trapped carriers are released from the localized tail states into the conduction band.[28]

Figure 2 shows a best fit to the photoexcitation and dark-relaxation data for the sampled illuminated with a λ of 400 nm. Figure 2(a) was re-plotted by the curve in Fig. 1 in order to extract the parameters through the stretched exponential fitting. Thus, the photo-conductivity in Fig. 2(a) was obtained by making use of following equation:

$$\sigma_{ph}(t) = \sigma_s - \sigma(t). \quad (5)$$

Here, $\sigma_{ph}(t)$ is the photo-conductivity in Fig. 2(a), σ_s is the saturation photo-conductivity which is the asymptotic conductivity at very long times, and $\sigma(t)$ is the measured photoconductivities with light illumination as shown in Fig. 1. The experimental data shown in Fig. 1 were fitted to the stretched exponential function to obtain the best fitting parameters such as β, τ, E_{ac} and Δ_{ac}. Table I summarizes the stretched exponential analysis, and the energy scales for activated behavior E_{ac} and Δ_{ac} are derived from an inverse Laplace transform analysis of these stretched exponentials.[11]

In the dark relaxation, the activation energy increased slightly as the wavelength increased. An increase of the activation energy means that relaxation occurs more slowly; therefore, τ is longer for the longer wavelength. Figure 3 shows the dark relaxation process for the various wavelengths. As the wavelength increases the relaxation time increases, which is coincident with the trend of the dark

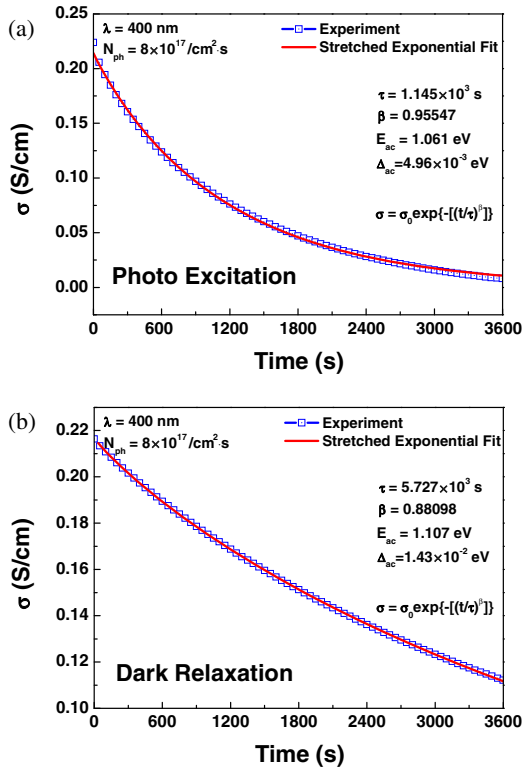

Fig. 2. (Color online) Typical conductivity vs time curve and its stretched exponential fit for (a) the photoexcitation and (b) dark-relaxation of the samples excited with $\lambda = 400\,\text{nm}$ and $N_{\text{ph}} = 8 \times 10^{17}/\text{cm}^2\cdot\text{s}$.

Table I. Summary of stretched exponential analysis. The values of parameters (β, τ, σ_s) are obtained from best fit to the data, and the energy scales for activated behavior, E_{ac} and Δ_{ac} are derived from inverse Laplace transform analysis of these stretched exponentials.[11)]

Photoexcitation						
λ (nm)	N_{ph} (/cm^2·s)	σ_s (S/cm)	β	τ (s)	E_{ac} (eV)	Δ_{ac} (eV)
400	4.02×10^{17}	0.281	0.9587	2.00×10^3	1.077	4.59×10^{-3}
400	6.04×10^{17}	0.306	0.9403	1.49×10^3	1.068	6.75×10^{-3}
400	8.05×10^{17}	0.459	0.9816	2.20×10^3	1.079	2.01×10^{-3}
400	8.00×10^{17}	0.2245	0.9555	1.15×10^3	1.061	4.96×10^{-3}
530	8.00×10^{17}	0.0223	0.9387	9.58×10^2	1.056	6.94×10^{-3}
850	8.00×10^{17}	0.0036	0.9766	8.32×10^2	1.052	2.56×10^{-3}
Dark-relaxation						
λ (nm)	N_{ph} (/cm^2·s)	σ_s (S/cm)	β	τ (s)	E_{ac} (eV)	Δ_{ac} (eV)
400	4.02×10^{17}	0	0.7515	6.43×10^3	1.110	3.44×10^{-2}
400	6.04×10^{17}	0	0.7542	6.26×10^3	1.109	3.39×10^{-2}
400	8.05×10^{17}	0	0.8540	2.67×10^3	1.085	1.80×10^{-2}
400	8.00×10^{17}	0	0.8810	5.73×10^3	1.107	1.43×10^{-2}
530	8.00×10^{17}	0	0.8787	2.26×10^4	1.146	1.46×10^{-2}
850	8.00×10^{17}	0	1.0000	3.03×10^4	1.155	—

relaxation activation energies for the various wavelength as shown in Table I. In Table I, the higher the value of β, the narrower the distribution of the dark relaxation becomes.[11)] A higher β value for a longer wavelength means that the metastable state for a longer wavelength has a narrower distribution than that for a shorter wavelength.

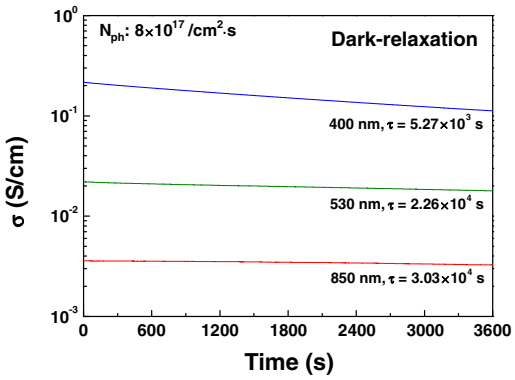

Fig. 3. (Color online) Dark-relaxation curves for various wavelengths with photon flux of $N_{\text{ph}} = 8 \times 10^{17}/\text{cm}^2\cdot\text{s}$.

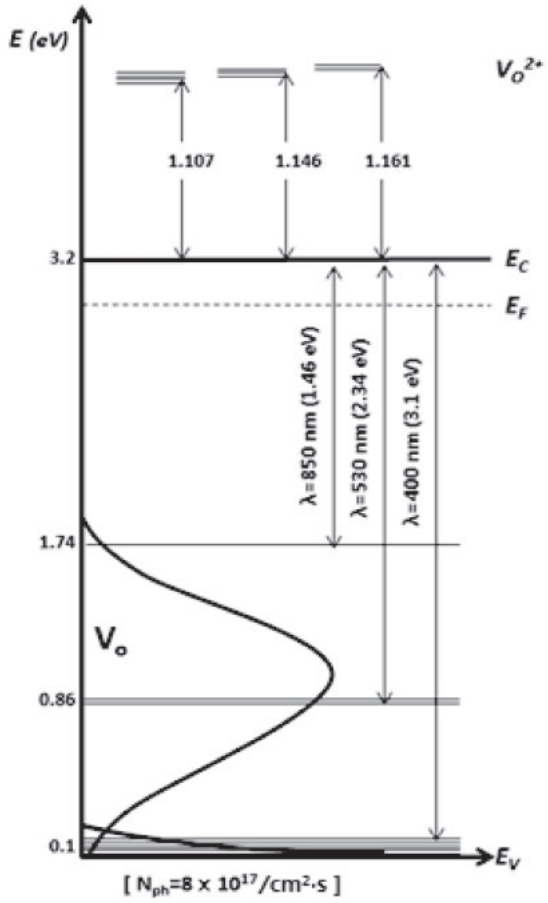

Fig. 4. Schematic energy band diagrams of light-treated a-IGZO thin films for dark-relaxation processes deduced from the experimental results for different wavelengths.

The wavelength dependency of the parameters shown in Table I suggest that the metastable state distribution by the light excitation is related to the distribution of oxygen vacancy state V_o,[29–31)] which is a rational expectation, because the different photon energies excite different energy levels' oxygen vacancies.

Figure 4 shows schematic energy band diagrams and the location of the ionized oxygen vacancies for each wavelength, based on the measurement results of the dark relaxation activation energy E_a and β. It shows that the

upper part of the oxygen vacancy V_o is ionized for the 850 nm wavelength. On the other hand, the shorter wavelengths are able to ionize oxygen vacancies deeply located near the valance band and oxygen vacancies shallowly located near the conduction band. For dark-relaxation, β closes to 1 as the wavelength increases, which means that the E_{ac} distribution becomes narrower for longer wavelengths.[11)]

The slow relaxation is not caused by the direct recombination of the photoelectrons and holes, but by the neutralization of the ionized vacancies. As many calculations show, the ionized vacancies are located above the bottom of the conduction band; the ionized oxygen vacancies are drawn above the bottom of the conduction band as shown in Fig. 4. We found several studies to support the idea that the ionized oxygen vacancies are located above the bottom of the conduction band. In studies by Noh et al.[25)] and Ryu et al.,[15)] it is explained that the V_o defects with the Ga–Ga bonds exhibit a high transition level above the bottom of conduction band with the hybrid density functional. In studies by Nahm et al.,[29,32)] it is explained that the calculated energy barrier was to be 2.9 and 3.9 eV through the simulation in peroxide state, and the fully-ionized V_o^{2+} state can be a metastable shallow donor state, since the defect level of V_o^{2+} is located above the bottom of the conduction band. This configuration can explain the slow relaxation of the dark current after illumination. The slow increase of the photoconductivity is due to the increase of the donor state, which is the ionized oxygen vacancy that appears above the bottom of the conduction band as shown in Fig. 4. The annihilation of the ionized oxygen vacancy is caused by the thermally excited electron from the conduction band.

For the longer wavelength, it shows higher relaxation activation energy; this means that the shallow-level vacancy forms a higher ionized energy level, and vice versa for the shorter wave length. Therefore, the shorter wavelength induces the wider distribution of the relaxation activation energy (smaller β value), because both the shallow-located oxygen vacancy and deep-located one can be ionized by the shorter wavelength.

4. Conclusions

The photo-response of a-IGZO was investigated for various wavelengths and intensities of light. The stretched exponential analysis was found to describe well both the photo-excitation and dark-relaxation characteristics. The decreases in τ and E_{ac} and the narrower distribution for the dark relaxation energy for the higher light intensity suggest that the meta-stable state distribution is related to the distribution of the oxygen vacancy state V_o.

With the incident light, a photo excitation process occurs and the oxygen vacancy is ionized to V_o^{2+} states which act as donors to increase the carrier density and are the origin of the slow photoexcitation. The V_o^{2+} states locate themselves above the conduction band edge (E_c), which is the origin of the slow dark-relaxation. During the dark relaxation, the time constant (τ) and the E_{ac} increase and the distribution of energy levels becomes narrower for longer wavelengths. The neutralization of V_o^{2+} to V_o becomes slower for longer wavelengths, due to the higher energy-barrier height (E_{ac}) for the neutralization of the V_o^{2+}.

Acknowledgement

This work was supported by the Industrial Strategic Technology Development Program (10041596, Development of core technology for TFT free active matrix addressing color electronic paper with day and night usage), funded by the Ministry of Trade, Industry, and Energy (MI, Korea).

1) K. Nomura, H. Ohta, A. Takagi, T. Kamiya, M. Hirano, and H. Hosono, Nature **432**, 488 (2004).
2) K. Nomura, H. Ohta, K. Ueda, T. Kamiya, M. Hirano, and H. Hosono, Science **300**, 1269 (2003).
3) K. Nomura, K. Ueda, H. Ohta, K. Ueda, M. Hirano, and H. Hosono, Appl. Phys. Lett. **85**, 1993 (2004).
4) T. Kamiya, K. Nomura, and H. Hosono, Phys. Status Solidi A **207**, 1698 (2010).
5) J. S. Park, W.-J. Maeng, H.-S. Kim, and J.-S. Park, Thin Solid Films **520**, 1679 (2012).
6) S.-H. K. Park, M. Ryu, S. Yang, S. M. Yoon, and C.-S. Hwang, J. Inf. Disp. **11** [3], 113 (2010).
7) D.-H. Cho, S.-H. K. Park, S. Yang, C. Byun, K. I. Cho, M. K. Ryu, S. M. Chung, W.-S. Cheong, S. M. Yoon, and C.-S. Hwang, J. Inf. Disp. **10** [4], 137 (2009).
8) D.-Y. Cho, J. W. Song, W. S. Choi, T. W. Noh, J.-Y. Kim, H.-G. Lee, B.-G. Park, S.-Y. Cho, S.-J. Oh, J. H. Jeong, Y.-G. Mo, and C. S. Hwang, Thin Solid Films **518**, 1079 (2009).
9) T. Sakai, H. Seo, S. Aihara, M. Kubota, N. Egami, D. Wang, and M. Furuta, Jpn. J. Appl. Phys. **51**, 010202 (2012).
10) H. Kitakado and S. Katoh, Jpn. J. Appl. Phys. **51**, 03CB02 (2012).
11) J. Luo, A. U. Adler, T. O. Mason, D. B. Buchholz, R. P. H. Chang, and M. Grayson, J. Appl. Phys. **113**, 153709 (2013).
12) T. Kamiya, K. Nomura, and H. Hosono, Sci. Technol. Adv. Mater. **11**, 044305 (2010).
13) H. Yabuta, M. Sato, K. Abe, T. Aida, T. Den, H. Kumomi, K. Nomura, T. Kamiya, and H. Hosono, Appl. Phys. Lett. **89**, 112123 (2006).
14) H. Hosono, J. Non-Cryst. Solids **352**, 851 (2006).
15) B. Ryu, H.-K. Noh, E.-A. Choi, and K. J. Chang, Appl. Phys. Lett. **97**, 022108 (2010).
16) W.-J. Lee, E.-A. Choi, J. Bang, B. Ryu, and K. J. Chang, Appl. Phys. Lett. **93**, 111901 (2008).
17) A. Takagi, K. Nomura, H. Ohta, H. Yanagi, T. Kamiya, M. Hirano, and H. Hosono, Thin Solid Films **486**, 38 (2005).
18) Y.-M. Kim, K.-S. Jeong, H.-J. Yun, S.-D. Yang, S.-Y. Lee, H.-D. Lee, and G.-W. Lee, Jpn. J. Appl. Phys. **51**, 09MF10 (2012).
19) H. Oh, S.-M. Yoon, M. K. Ryu, C. S. Hwang, S. Yang, and S.-H. K. Park, Appl. Phys. Lett. **97**, 183502 (2010).
20) D. H. Lee, K.-I. Kawamura, K. Nomura, T. Kamiya, and H. Hosono, Electrochem. Solid-State Lett. **13**, H324 (2010).
21) S.-H. K. Park, M. Ryu, S. M. Yoon, S. Yang, C.-S. Hwang, J.-H. Jeon, and K. Kim, Jpn. J. Appl. Phys. **50**, 03CB08 (2011).
22) P. Görrn, M. Lehnhardt, T. Riedl, and W. Kowalsky, Appl. Phys. Lett. **91**, 193504 (2007).
23) H. C. Oh, S. M. Yoon, M. K. Ryu, C. S. Hwang, S. H. Yang, and S.-H. K. Park, Appl. Phys. Lett. **98**, 033504 (2011).
24) M. D. H. Chowdhury, P. Migliorato, and J. Jang, Appl. Phys. Lett. **97**, 173506 (2010).
25) H.-K. Noh, K. J. Chang, B. Ryu, and W.-J. Lee, Phys. Rev. B **84**, 115205 (2011).
26) J. H. Kim, U. K. Kim, Y. J. Chung, and C. S. Hwang, Appl. Phys. Lett. **98**, 232102 (2011).
27) K. Ghaffarzadeh, S. S. Lee, A. Nathan, J. Robertson, S. H. Jeon, S. W. Kim, C. J. Kim, U.-I. Chung, and J.-H. Lee, SID Symp. Dig. Tech. Pap. **42**, 1154 (2011).
28) S. Yasuno, T. Kita, S. Morita, T. Kugimiya, K. Hayashi, and S. Sumie, J. Appl. Phys. **112**, 053715 (2012).
29) H.-H. Nahm, Y.-S. Kim, and D. H. Kim, Phys. Status Solidi B **249**, 1277 (2012).
30) T.-C. Fung, C.-S. Chuang, K. Nomura, H.-P. D. Shieh, H. Hosono, and J. Kanicki, J. Inf. Disp. **9** [4], 21 (2008).
31) K. W. Lee, H. S. Shin, K. Y. Heo, K. M. Kim, and H. J. Kim, J. Inf. Disp. **10** [4], 171 (2009).
32) H.-H. Nahm, C. H. Park, and Y.-S. Kim, Sci. Rep. **4**, 1038 (2014).